Washington University in St. Louis
Washington University Open Scholarship

McKelvey School of Engineering Theses & Dissertations
McKelvey School of Engineering

Winter 12-2023

Enhanced Fabrication of Microdroplet Generator Nozzle Arrays: Optimizing KOH Etching for Microfluidic Applications

Hongyu Bai

Follow this and additional works at: https://openscholarship.wustl.edu/eng_etds

Part of the Mechanical Engineering Commons

Recommended Citation
Bai, Hongyu, "Enhanced Fabrication of Microdroplet Generator Nozzle Arrays: Optimizing KOH Etching for Microfluidic Applications" (2023). *McKelvey School of Engineering Theses & Dissertations*. 986.
https://openscholarship.wustl.edu/eng_etds/986

This Thesis is brought to you for free and open access by the McKelvey School of Engineering at Washington University Open Scholarship. It has been accepted for inclusion in McKelvey School of Engineering Theses & Dissertations by an authorized administrator of Washington University Open Scholarship. For more information, please contact digital@wumail.wustl.edu.

WASHINGTON UNIVERSITY IN ST. LOUIS

McKelvey School of Engineering
Department of Mechanical Engineering & Materials Science

Thesis Examination Committee:
Mark Meacham, Chair
Xianglin Li
Patricia Weisensee

Enhanced Fabrication of Microdroplet Generator Nozzle Arrays: Optimizing KOH Etching for Microfluidic Applications

by
Hongyu Bai

A thesis presented to
the McKelvey School of Engineering
of Washington University in
partial fulfillment of the
requirements for the degree
of Master of Science

December 2023
St. Louis, Missouri

© 2023, Hongyu Bai

Table of Contents

List of Figures iii
Acknowledgments v
Abstract vi
Chapter 1: Background and State of Practice 1
1.1 Introduction 1
1.2 Chip Fabrication 3
1.3 KOH Etching and Reactive Ion Etching (RIE) 7
1.4 Problems and Limitations 8
1.5 Ultrasonic Wet Etching 9
Chapter 2: Methodology 10
2.1 Test Wafer Design 10
2.2 Photolithography 11
2.3 Wet Etching 12
Chapter 3: Results 15
3.1 Results of Selectivity 15
3.2 Geometry of the Pyramid 15
3.3 Observed Issues and Possible Sources of Error 23
3.4 Surface Morphology 25
Chapter 4: Conclusions 29
References 32

List of Figures

Figure 1.2.1 Illustration of fabrication procedure……………………………..………4

Figure 1.2.2 KOH etching with stirring bar…………………………………….……5

Figure 2.1.1 (a) The CAD design of the testing features. (b) Dimension of microarrays from 615μm to 665μm. (c) Detailed view of side line squares from 590μm to 640μm with increments of 5μm…………………………………...………………………..10

Figure 2.3.1. (a) Detailed view of picked square for each measured microarray. (b) Detailed view of picked square for measurement….…………………………...……..13

Figure 2.3.2. Illustration of measured parameters of the pyramid/ trapezoid during the KOH etching……………………………………………………………………..…14

Figure 3.2.1. Average Etch Depth Rate (µm/hours) of Various Feature Sizes at 70°C Over Etching Time. This figure illustrates the relationship between the etching time and the average depth etch rate for different sizes of etched features………………………..17

Figure 3.2.2. Average Etch Depth Rate (µm/hours) of Various Feature Sizes at 65°C Over Etching Time. This figure illustrates the relationship between the etching time and the average depth etch rate for different sizes of etched features………………………..17

Figure 3.2.3. Comparative Analysis of Average Expansion Rates for Squares on the Silicon Nitride Layer Across Different Feature Sizes. This graph displays two sets of data: the blue bars represent the expansion rates achieved using KOH etching at 70°C, while the red bars illustrate the expansion rates for KOH etching at 65°C…………...…18

Figure 3.2.4. Average Depth for microarrays at varied distances from the wafer's center at 65°C. This figure demonstrates the variation in the average depth etch rate of microarrays……………………………………………………………………………18

Figure 3.2.5. Average Depth etching rates for microarrays at varied distances from the wafer's center at 65°C. This figure demonstrates the variation in the average depth etch rate of microarrays……………………………………………………………...…..19

Figure 3.2.6: Anomalies Observed During KOH Etching at 65°C. (a) displays the problematic wafer at 65°C, where concentric wave patterns are visible within the red circle, discernible to the naked eye due to variations in the refraction angle and refractive index. (b) shows the appearance of the upper layer under a microscope at 2.5×

magnification. (c) depicts the bottom layer as observed under 20 × magnification through the microscope…………………………………………………………………...…20

Figure 3.2.7: This figure illustrates the dimensional changes at the bottom of the nozzle over the course of KOH etching time. The blue curve represents the etching progression at 65°C, while the red curve denotes the changes observed at 70°C…………………….21

Figure 3.2.8: This figure illustrates the dimensional changes at the top of the nozzle over the course of KOH etching time. The blue curve represents the etching progression at 65°C, while the red curve denotes the changes observed at 70°C……………………….22

Figure 3.2.9: Ripple-patterned wafer surface, exhibiting a diffusion-like spread from the center……………………………………………………………………………...…22

Figure 3.4.1. Surface Morphology of the Side Wall on the (111) Plane of 75ºC KOH etching. (a) in the X-direction and (b) in the Y-direction………………………………..25

Figure 3.4.2. Surface Morphology of the Side Wall on the (111) Plane of 70ºC KOH etching. (a) in the X-direction and (b) in the Y-direction………………………………..26

Figure 3.4.3. Surface Morphology of the Side Wall on the (111) Plane of 65ºC KOH etching. (a) in the X-direction and (b) in the Y-direction………………………………..26

Figure 3.4.4. This figure presents the varying surface morphologies of the silicon nitride layer post-KOH etching at different temperatures for a feature size of 645µm. (a) represents the surface after the KOH etching of 75°C, (b) 70°C, and (c) 65°C………....27

Figure 3.4.5: Pyramid Tips Resulting from KOH Etching at 65°C…………………...…28

Acknowledgments

First, I would like to thank my parents and family for their unconditional love and support throughout my study life. All of my achievements could not have been possible without their strong support.

I want to thank my professors and lab managers for their guidance, which has significantly contributed to my academic growth. Special thanks to Dr. Mark Meacham, Dr. Kashif Awan, and Dr. Liangji Zhang for their invaluable advice and support.

Thanks to my lab mates for their encouragement and valuable insights throughout our time together at the university. Thank you, Andreea, Aaron, Advaith, and Nirvan. My delightful master's study experience is all thanks to them.

I would like to express my appreciation to my committee for their guidance. Thank you, Dr. Xianglin Li, Dr. Patricia Weisensee, and Dr. Mark Meacham, for your time and invaluable insights throughout my research.

Up to this point, words are not enough to express all my feelings. I will stay on my path and never give up.

Hongyu Bai

Washington University in St. Louis

December 2023

ABSTRACT OF THE THESIS

Enhanced Fabrication of Microdroplet Generator Nozzle Arrays: Optimizing KOH Etching for Microfluidic Applications

by

Hongyu Bai

Master of Science in Mechanical Engineering

Washington University in St. Louis, 2023

Professor John Mark Meacham, Chair

Ultrasonic microdroplet generators are useful devices with broad applications ranging from aerosolized drug delivery to three-dimensional (3D) printing-based additive manufacturing. One such technology comprises a microfabricated array of nozzles with droplet production driven by a piezoelectric transducer. The present study focuses on refining a critical fabrication step, anisotropic wet etching of pyramidal nozzles using a basic potassium hydroxide (KOH) solution. Given the integral role of nozzle geometry in device operation, high-precision techniques including Reactive Ion Etching (RIE), Deep Reactive Ion Etching (DRIE), and KOH wet etching were employed. A tapering geometry is preferred for acoustic wave focusing and efficient droplet generation, and KOH etching naturally yields pyramids due to preferential removal of the (100) plane versus the (111) plane of single-crystal silicon. Though wet etching is less precise than dry etching, it is difficult to form these 3D shapes using dry etching alone. Thus, this work focused on realizing the highest possible level of control over KOH etching. Challenges were encountered in using a conventional etching setup to achieve uniform

etching and good surface smoothness, which are crucial to definition of the pyramidal tip geometry. These aspects are also important for use of KOH etching to define microstructures in a range of microfluidic systems. Here, we introduce an ultrasonic-assisted etching method to enhance the KOH etching process, addressing issues like non-uniform etching rates and surface roughness. This research not only provides insight into the microfabrication of ultrasonic microdroplet generators but also contributes to further improvements in microfluidic device manufacturing.

Chapter 1: Background and State of Practice

1.1 Introduction

Microfluidic devices with controllable liquid dispensing, specifically those that can produce uniform droplets, have great potential in many technological applications, such as traditional manufacturing [1]-[2], the chemical industry [3]-[4], biology/biomedicine [5]-[7], thermal management [9]-[11], and three-dimensional (3-D) printing [12]-[13]. The controlled generation of droplets, in terms of size, size distribution, frequency, velocity, and composition, is foundational for applications ranging from high-throughput screening in drug discovery to advanced materials synthesis. Within this context, the acoustic microfluidic droplet generator stands out for its unique droplet formation mechanism.

Ultrasonic devices utilize sound wave energy instead of traditional droplet generators that depend on hydrodynamic flow inconsistencies at microchannel intersections. In this context, piezoelectric actuators produce periodic vibrations, injecting acoustic power into liquid chambers. This action results in pressure peaks and troughs in the liquid, prompting the formation of droplets at specific drive voltages and frequencies.

Many possible nozzle geometries could be envisioned; however, the pyramidal structure is applied widely due to straightforward manufacture of such silicon nozzle microarrays using anisotropic wet etching. The pyramid shape was first applied by Diepold et al. who reported an inkjet printer head that produced a continuous stream of droplets. Palm et al. published research on a droplet generator with single square orifices, demonstrating

enhanced stability of a train. The fabrication of the ultrasonic droplet generator described in the present research is based on Meacham et al. [14]. The design and fabrication process were further discussed and analyzed by Li et al. [15] The performance of the micromachined ultrasonic droplet generator not only depends on the input voltage and frequency, but also on the geometrical parameters, such as orifice size, pyramid structure, and the surface characteristic of the pyramids. Although the geometrical parameters were not a major factor in dictating pressure distributions, the spray characteristics were significantly influenced by the size and exit orifice shape of the pyramids [15].

The primary focus of this study revolves around the fabrication of ultrasonic droplet generators. Drawing from prior research, techniques employed in this study encompass reactive ion etching (RIE), deep reactive ion etching (DRIE), and potassium hydroxide (KOH) wet etching. In order to open square windows on the silicon wafer with silicon nitride coating, ion beam etching, phosphoric acid etching, and RIE etching are three feasible methods. Considering time, complexity, and expense, RIE etching is a reliable method compared to ion beam etching which and phosphoric acid etching during the mask layer processing. The pyramid nozzles were made by KOH etching which has a much lower etching rate over the <111>plane comparing to the <111> plane of the silicon substrate. However, the conventional KOH etching method struggled to etch the silicon wafer coated with silicon nitride uniformly and nozzle size expansion, especially when aiming for a smooth surface. Here, an ultrasonic cleaner was used to improve the KOH etching process by uniformly removing hydrogen gas bubbles liberated during the etch process. This helped to eliminate local masking to yield a smoother surface.

1.2 Chip Fabrication

For basic control of droplet size and ejection mode (continuous jet or discrete droplet), we made nozzle microarrays with three different orifice diameters: 10, 20, and 40 μm. We began with a double-side polished silicon substrate [(100)-oriented, 100-mm diameter, 500- μm thick; University Wafer] precoated on both sides with a silicon nitride (Si_3N_4) masking layer [~ 650-nm thick, low pressure chemical vapor deposited (LPCVD); Georgia Institute of Technology Institute for Electronics and Nanotechnology][15].

As illustrated in Figure 1.2.1[22], the blue layer represents silicon nitride (Si_3N_4), the gray layer signifies silicon, and the red layer denotes photoresist.

The first step of the fabrication process was spin-coating the photoresist (S1827) on the nitride-coated silicon wafer. If the wafer was not clean, a cleaning process was required. The standard procedure was to clean the wafer with acetone, isopropyl alcohol (IPA) and DI water. Using nitrogen gas to dry the wafer. The wafer was then put on a hotplate at 115 °C for 10 minutes. The silicon wafer was spin-coated with a 4μm layer of the photoresist (S1827). The square array pattern was written into the resist film by the Heidelberg laser writer DWL 66+. After exposure to ultraviolet laser light, the photoresist on the wafer was developed in MF-319 developer for about 2.5 minutes. Then, the wafer was rinsed with DI water immediately to stop the development process and cleaned with nitrogen gas. The remaining resist film was then hard baked on the hotplate for 5 minutes at 110 °C to improve its resistance to etching in the reactive ion etcher.

Reactive ion etching (RIE) was used to create square windows on the front side of the wafer as prescribed by the pattern in the photoresist film. The recipe used for silicon nitride etching took about 5 minutes to etch through the thin layer of silicon nitride.

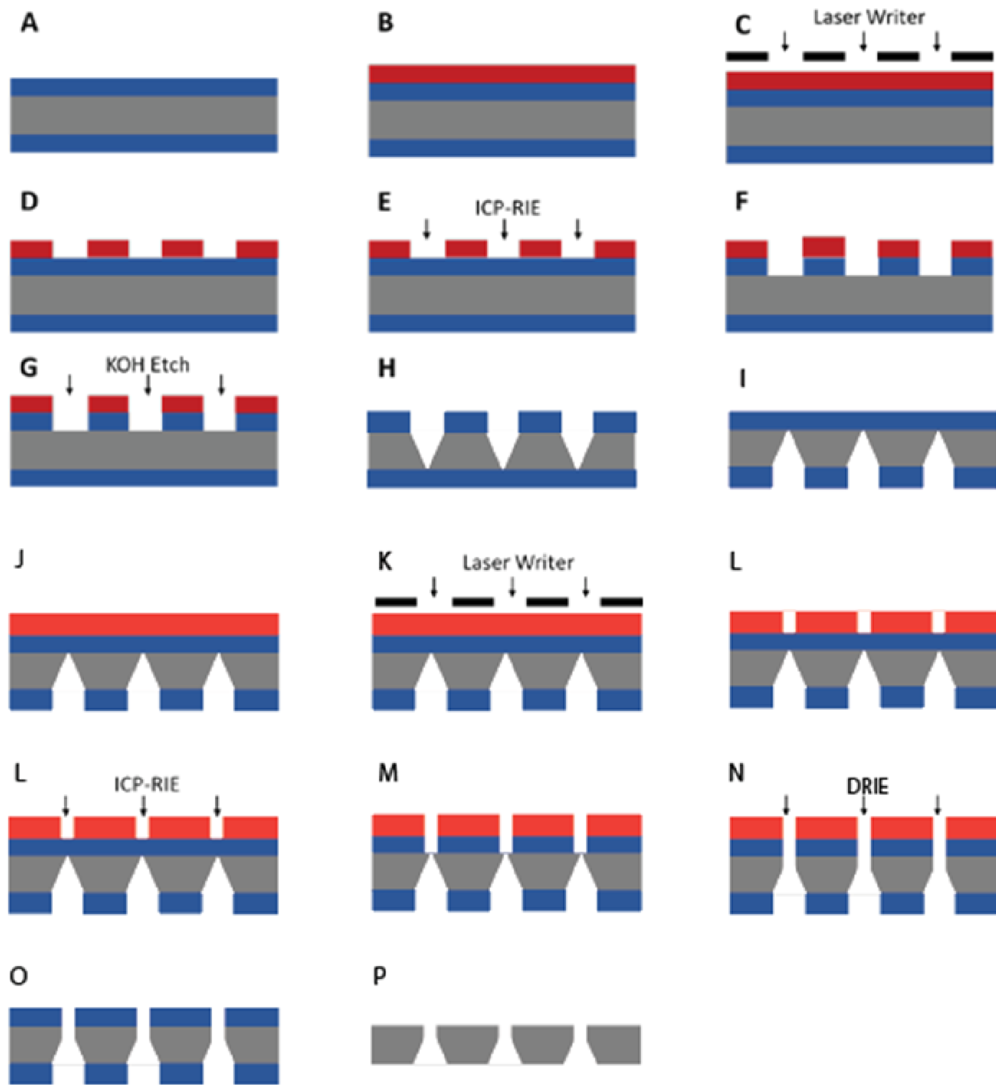

Figure 1.2.1. Illustration of fabrication procedure.

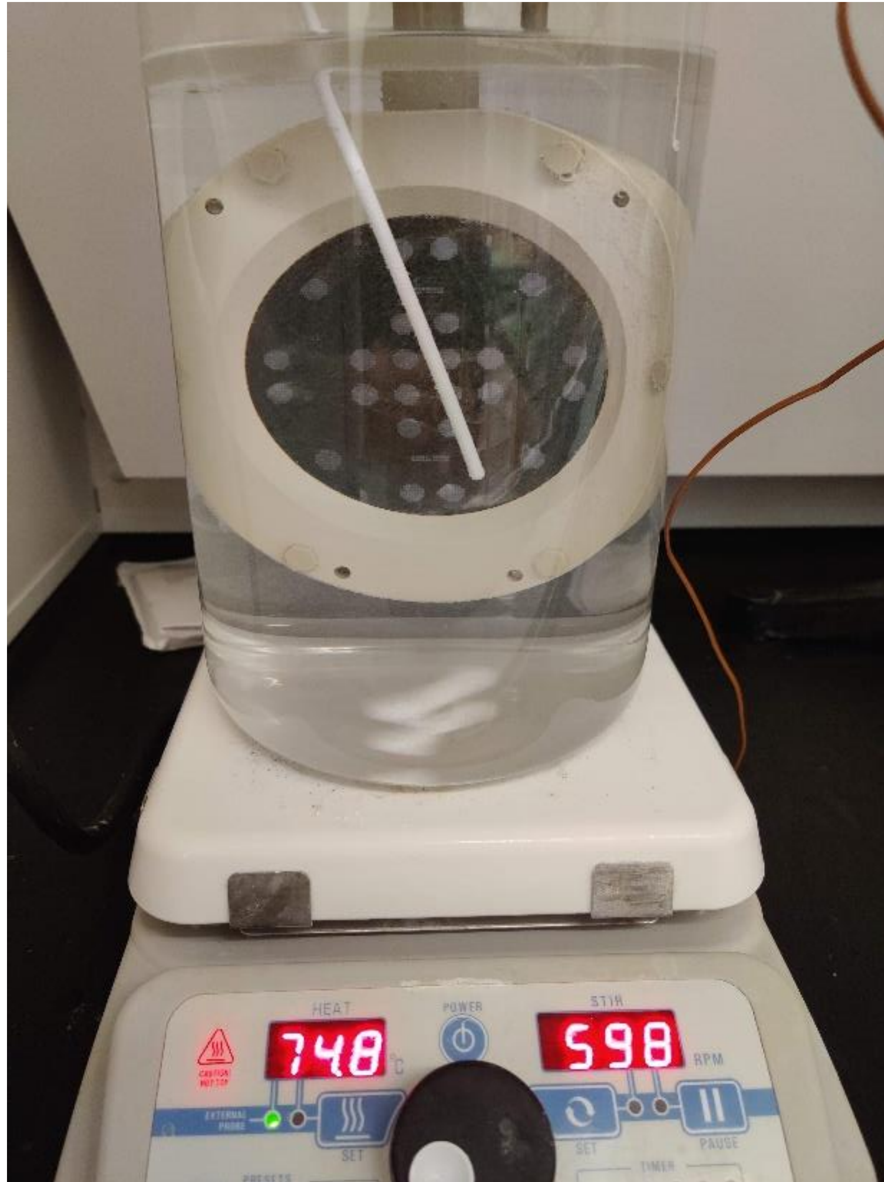

Figure 1.2.2. KOH etching with stir bar.

The fabricated wafer was mounted in a polyether ether ketone (PEEK) holder for KOH etching. The holder was designed to protect the backside of the wafer from attack by the solution. For conventional etching of the pyramidal nozzle microarrays, the KOH solution (LOT 193337, Fisher Chemical) was poured in a large quartz beaker, as shown in Figure 1.2.2, and pre-heated until the solution temperature stabilized at 75°C. A

magnetic stir bar was place in the KOH solution with stirring rate at 600 RPM to agitate the solution and remove liberated hydrogen gas during the etch.

To summarize, the project used (i) standard photolithography to create the design patterns, (ii) reactive ion etching (RIE) to create square windows in the nitride film, and (iii) anisotropic potassium hydroxide (KOH) wet etching of the silicon to form pyramids. For the orifices at the tip of the nozzles, we relied on back side alignment and deep reactive ion etching (DRIE) of any remaining silicon at the nozzle tips to form circular orifices.

1.3 KOH Etching and Reactive Ion Etching (RIE)

In the domain of silicon microfabrication, the etching technique selected critically influences the final surface features of a microchip or device. For device necessitating both smooth surfaces and pyramidal structures, it is imperative to delve into the nuances of potential etching methods, particularly KOH wet etching and reactive ion etching (RIE).

RIE is the common technique used in the industry. The fundamental distinction in RIE lies in its anisotropic etching capability, with the ability to deliver a much higher etching rate and more adjustable selectivity than the KOH etching.

In comparison, KOH wet etching offers a natural advantage when it comes to etching silicon. This method exploits the inherent differences in etch rates of silicon's crystallographic planes. Specifically, in the presence of a KOH solution, the (100) planes are etched much faster than the (111) planes. This differential etch rate leads to the formation of pyramidal structures based on the intrinsic crystallographic character of the silicon, making it a favorable technique for this project.

Additionally, the uniform etching profile provided by the liquid-phase method in KOH wet etching results in smoother surface finishes, which aligns well with the project requirements. Conversely, RIE, due to its ion bombardment, has the potential to introduce unintended roughness to the silicon surface [16].

When considering the equipment needed, KOH wet etching requires less intricate equipment compared to RIE, potentially leading to cost and process simplifications. Considering these insights, it can be deduced that for applications aiming for pyramidal

structures and smoother surface finishes, KOH wet etching presents many inherent advantages over RIE.

1.4 Problems and Limitations

Although KOH etching can essentially meet the basic requirements of the project, we encountered some issues. During the previous preparation process, the KOH solution was introduced into a large beaker placed on a hotplate. To ensure precise temperature control, a thermocouple was attached to the hotplate and submerged in the KOH solution. Additionally, the magnetic stir bar was placed in the solution.

However, while the combination of hotplate and magnetic stirring provided good uniformity of the temperature within the beaker containing the KOH, the sizes of the resulting pyramidal features and the smoothness of their surfaces were not at the desired level on a consistent basis (i.e., across features on a single wafer or from wafer to wafer etched in the same way).

In microfluidic systems, the precision of channel and microstructure dimensions is crucial for accurate flow control and in our case, droplet formation. Any non-uniformity in KOH etching can lead to dimensional deviations in microstructures, which will directly affect the size and size distribution of droplets. This uniformity is particularly essential in applications such as drug delivery, chemical reactions, and bioassays, where the consistency of droplet volume is necessary to ensure the repeatability and accuracy of experimental outcomes. Maintaining a smooth surface finish and managing flow rates are therefore essential to achieving predictable and stable droplet ejection in such devices [20]-[21].

1.5 Ultrasonic Wet Etching

During the KOH etching with a magnetic bar, gas bubbles generated from the surface of features. The reaction between KOH and silicon produces silicate and hydrogen gas. The hydrogen gas forms bubbles which adhere to the surface of the silicon wafer. The adhesion of gas bubbles will lead to a varying etching rate at different areas of the silicon wafer.

According to the review by Pal et al., employing ultrasonic agitation during KOH etching of silicon notably enhances the etch rate while simultaneously improving the surface morphology. Moreover, the vibrations produced by the ultrasonic waves are beneficial in enhancing the quality of the etched surface. The use of ultrasonic energy facilitates the removal of adhered hydrogen gas bubbles, thus improving the contact between the etching surface and the KOH solution. [17]

The operation of ultrasonic KOH etching necessitates heating the beaker of KOH solution in a water bath tank, ensuring uniform temperature distribution during the etching process. This approach provides a more stable etching rate throughout, which reduces the upper layer expansion rate and ensures that the feature size meets the design parameters. This improvement in the experimental procedure could ensure that fabricated microarrays meet desired geometries to allow further characterization and optimization of the ultrasonic droplet generator performance.

Chapter 2: Methodology

2.1 Test Wafer Design

The microfeatures were designed based on a 4-inch wafer, with each color in Figure 2.1.1 (a) denoting a distinct square array size. The size of squares in each nozzle arrays were range from 615µm to 665µm. The size of the features was chosen to examine the etch rate of the upper layer of the nozzle. The linear arrangement of square arrays shown in Figure 2.1.1 (c) represents sizes that range from 590µm to 640µm, alignment features in the original design, with each successive array increasing by an increment of 5µm.

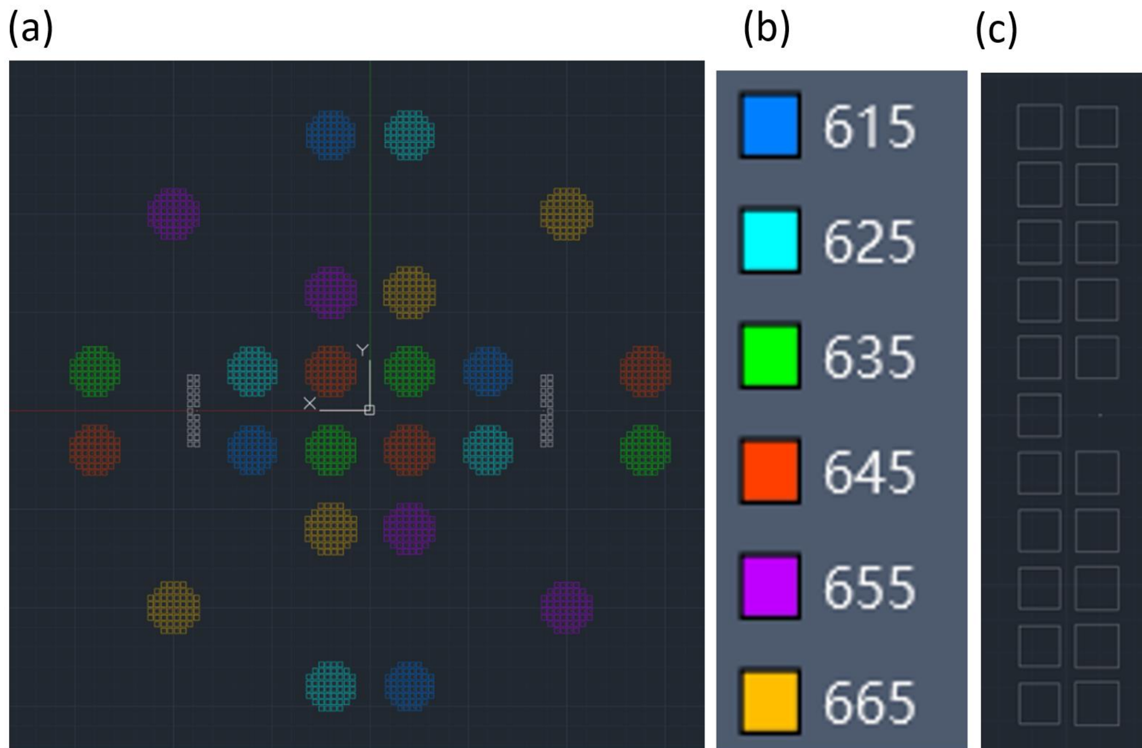

Figure 2.1.1. (a) The CAD design of the testing features. (b) Dimension of microarrays from 615µm to 665µm. (c) Detailed view of side line squares from 590µm to 640µm with increments of 5µm.

The above design allows for a precise analysis of size-dependent variations in the etching process.

2.2 Photolithography

The spin coating of photoresist is the primary step that influences the results of exposure and feature development in the lithographic processes. To enhance the lithography results, this study introduced the use of a primer prior to the application of the photoresist. The primer was applied to enhance the adhesion between the photoresist and the substrate and to modify the substrate surface to become more compatible with the photoresist. Additionally, the application of primer also contributes to a better compatibility of positive photoresist, S1827, which improved the critical dimension control during the photolithography process.

During the fabrication process, the use of primer was found to affect the photoresist spin coated on the silicon nitride layer, inadvertently leading to overexposure during the laser writing. To solve this issue, a dose test was executed using the calibration matrix function on the Heidelberg laser writer operation program. The original settings for the photoresist S1827 were: Focus at 0%, Intensity at 100%, Laser Power at 70mW, and Filter at 100%. Post-dose testing, the microscope observations indicated that the best result was made with the following adjusted parameters: Focus at -25%, Intensity at 60%, while maintaining the Laser Power at 70mW and the Filter at 100%.

In this study, three wafers were applied. The thickness of silicon nitride layers coated should be 600nm, however, the actual thickness for wafers used were not identical. Wafer 1 for 75°C ultrasonic KOH etching is 524.6 µm. The thickness of wafer 2 is 524.8 µm for 70 °C etching, and wafer 3 524.6 µm for 65°C etching. The RIE time for the first wafer, had an etching time of 5 minutes, and the DC bias during the RIE was 183V. The second

wafer was etched for 7 minutes with DC bias at 190V. The etching time was 5+1 minutes at 193V DC bias for the third wafer.

$$S_e = \frac{R(A)}{R(B)} \tag{2.2.1}$$

In above equation (2.2.1), S is selectivity, R(A) is the etch rate of silicon nitride masking layer, and R(B) is the etch rate of photoresist S1827.

2.3 Wet Etching

KOH etching inherently produces pyramidal structures due to the preferential removal of the (100) plane over the (111) plane in single-crystal silicon. However, under varying concentrations, temperatures, and other conditions, the etching rates of the (100) and (111) planes and the structural changes induced by etching cannot be determined through simple calculations without performing experimental characterization of the etch process. To calibrate the KOH etching of silicon wafers coated with silicon nitride, three wafers mentioned in section 2.2 were used in this study. This was done to negate any potential effects of silicon thickness and the silicon nitride mask on the test results.

Therefore, changes in dimensions of features during the etching process under different temperature conditions were measured. In this project, the Fisherbrand FB11207 ultrasonic cleaner was utilized to facilitate ultrasonic KOH etching. The KOH solution employed was a 45% w/v solution from Thermo Fisher Scientific Throughout the process, the ultrasonic cleaner was set to maintain 40 watts and an ultrasonic frequency of 80 kHz. The detailed data for wafers tested at 70°C and 65°C were meticulously recorded for comparison and analysis, including metrics like etching rate and expansion

rate. Additionally, photographs capturing the surface characteristics of three wafers were taken for comparative purposes.

For each circular nozzle array corresponding to a nozzle size (i.e., discrete base sizes of 615µm, 625µm, 635µm, 645µm, 655µm, and 665µm), two of four arrays were selected for measurement, resulting in a total of 12 circular nozzle arrays being evaluated, as shown in Figure 2.3.1(a) For each circular array, several fixed squares (nozzles) were selected for measurement to ensure the reliability of the data. In the side line, two of each size were also picked for measurement, as labeled in Figure 2.3.1(b).

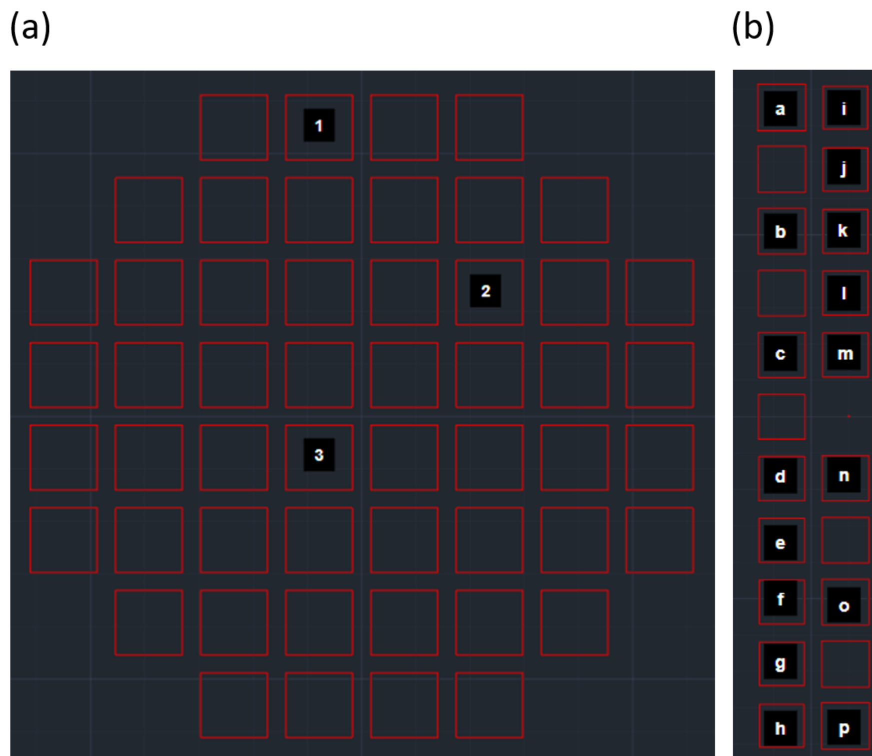

Figure 2.3.1. (a) Detailed view of picked square for each measured microarray. (b) Detailed view of picked square for measurement.

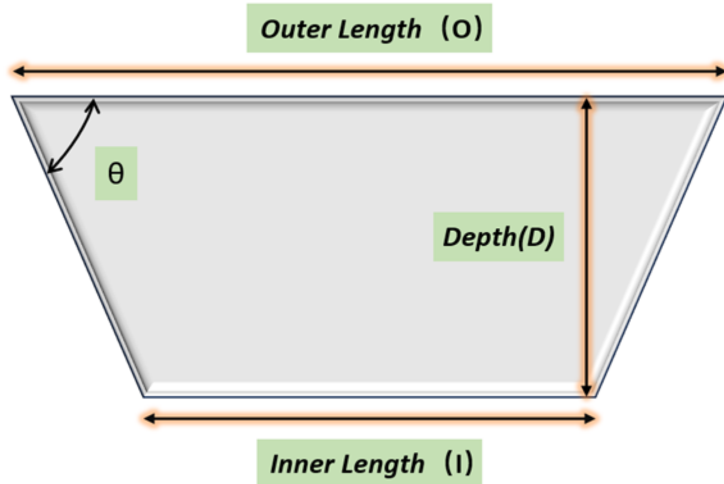

Figure 2.3.2. Illustration of measured parameters of the pyramid/ trapezoid during the KOH etching

$$\text{Angle:}\theta = tan^{-1}[\frac{D}{(0.5\times(O-I))}] \quad (2.3.1)$$

Figure 2.3.2 provides a detailed view of the various parameters that require measurement. The 'Outer Length' (O) is size of square on the silicon nitride layer, while the 'Inner Length' (I) denotes the length of bottom area of the etched feature. The angle of the side wall from (100) surface to the (111) plane was calculated by equation (2.3.1).

The lengths were determined using a Zeiss Axiovert microscope, equipped with Zeiss's ZEN microscopy software. Images of each feature were captured after zooming to a suitable scale, and the lengths were then measured from these images using the distance function in the software. To measure the etching depth, the focus point on the top layer was established as the zero position. The microscope focus was then moved towards the bottom of the etched feature. The depth was indicated by the *z*-position displayed on the microscope's readout.

Chapter 3: Results

3.1 Results of Selectivity

The calculation of selectivity between photoresist s1827 and silicon nitride was determined as follows. For the third wafer the average depth before RIE was 2955 nm, 2775 nm after RIE, and 577 nm with photoresist removed. The duration of RIE etching was 6 min. According to the calculation (3.1.1), the selectivity for wafer 3 is,

$$s = \frac{(2775-577) \div 360}{(2955-2775) \div 360} = 12.21 \qquad (3.1.1)$$

The selectivity for the second wafer was 12.98, and 12.25 for the first wafer.

3.2 Geometry of the Pyramid

Measurements of the features were conducted every two hours, and the results were calculated and statistically analyzed using Equation (2.3.1). The average slide wall angles for KOH etching at 75°C, 70°C, and 65°C were found to be 55.89, 56.10, and 55.73 degrees, respectively, which is extremely close to the known angle between (111) and (100) planes of single crystal silicon, 54.74 degrees. The standard deviation for the data at 75°C was 1.32, at 70°C it was 4.1, and at 65°C it was 1.19. Given that these results were derived from only three measurements, they exhibit significant variability and should be interpreted with caution. They are indicative rather than definitive, primarily serving to assess the consistency of the etching results. For more precise determination of the side wall angles, it is necessary to dice the wafer and measure the cross-sectional angles, which would yield more accurate values.

Ultrasonic KOH etching at 70ºC and 65 ºC were used to characterized the effect of temperature on the designed microarrays, and 75ºC etching was used to exam the fabrication operation process.

The KOH etching rate at 70°C exhibited a linear decrease over the period from 2 to 12 hours. During this time, some features that had already developed into pyramidal shapes continued to experience a declining etching rate. It appears that all measurements suggest declining etch rates with time even before any of the pyramids could have terminated. Even at 4 hours, the etch rate is lower than at 2 hours, and it continues to decrease steadily before the etch could possibly be done for any of the features. Conversely, other features that had not yet fully formed into pyramids at 12 hours displayed a slight increase in their etch rates. In contrast, the KOH etching at 65°C, spanning from 2 to 16 hours, exhibited a largely stable rate, with the minimum and maximum values being 19.82 and 34.43, respectively. At the wafer's edges, some microarrays formed complete pyramid shapes around 16-18 hours, whereas near the center, the pyramids of many microarrays remained unformed. In these central microarrays, the depth etching rate initially increased between 16 to 18hours and then rapidly declined after 18 hours.

Based on Figures 3.2.1 and 3.2.2, it can be generally concluded that KOH etching at 65°C exhibits a lower depth etching rate compared to the etching process conducted at 70°C. Simultaneously, as observed in Figure 3.2.3, a comparison between the etching processes at 65°C and 70°C reveals that the expansion (i.e., etching of the (111) crystal plane) of features at the upper surface of the silicon, namely the silicon nitride layer, is significantly less at 65°C for all base sizes. The difference in the maximum expansion

rates between these two temperatures is 6.81µm/hour, while the smallest observed difference is 4.28µm/hour.

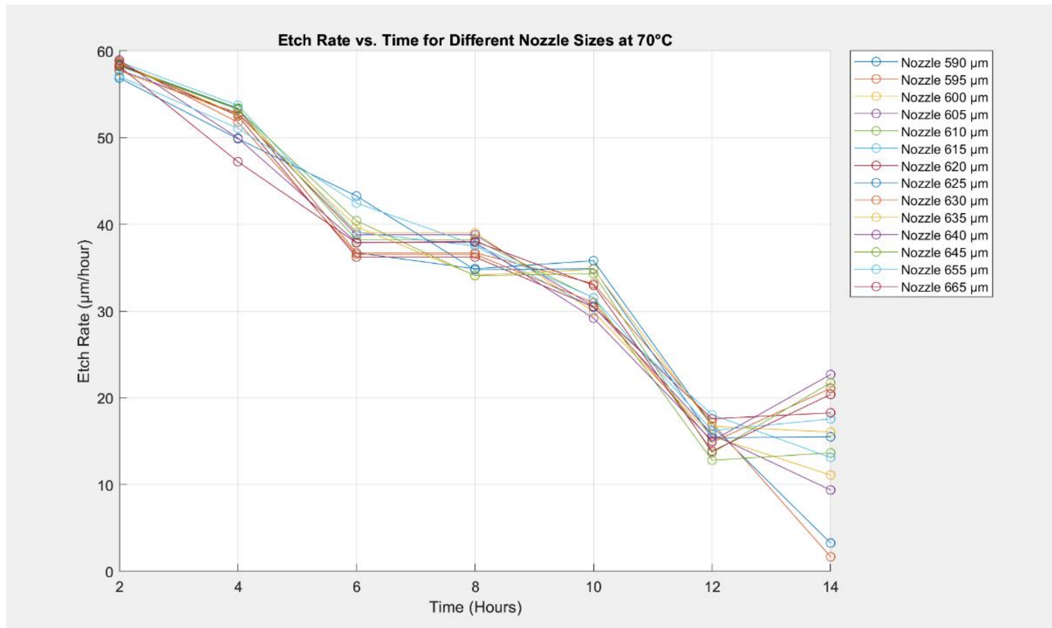

Figure 3.2.1. Average Etch Depth Rate (µm/hours) of Various Feature Sizes at 70°C Over Etching Time. This figure illustrates the relationship between the etching time and the average depth etch rate for different sizes of etched features.

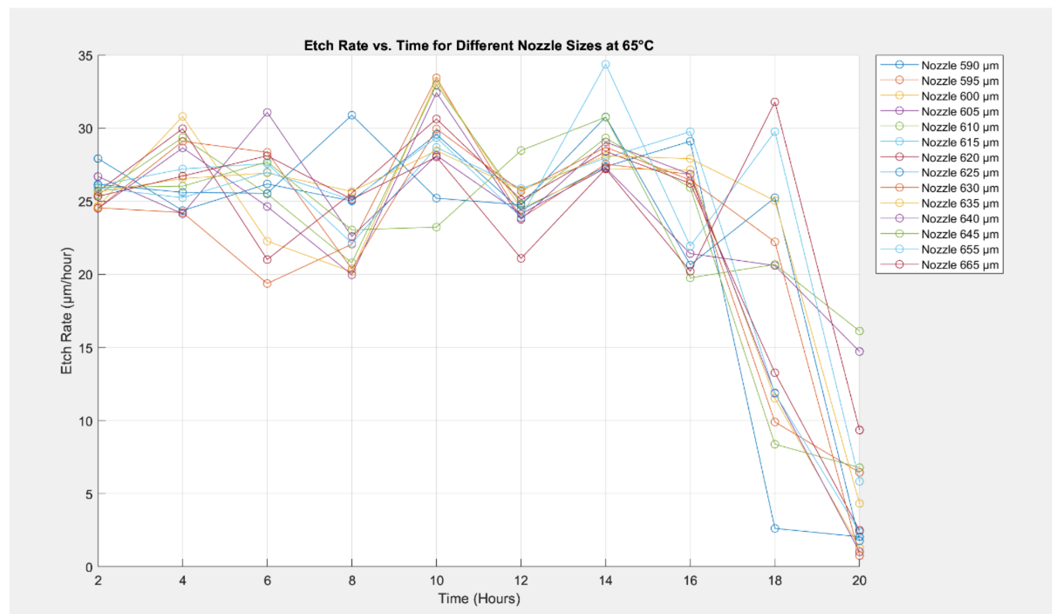

Figure 3.2.2. Average Etch Depth Rate (µm/hours) of Various Feature Sizes at 65°C Over Etching Time. This figure illustrates the relationship between the etching time and the average depth etch rate for different sizes of etched features.

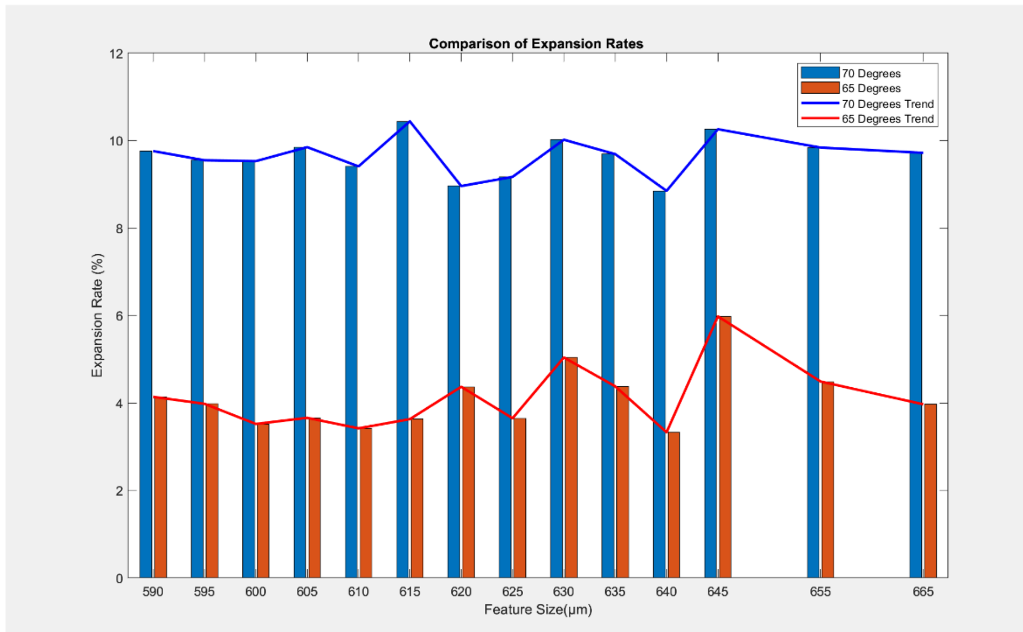

Figure 3.2.3. Comparative Analysis of Average Expansion Rates for Squares on the Silicon Nitride Layer Across Different Feature Sizes. This graph displays two sets of data: the blue bars represent the expansion rates achieved using KOH etching at 70°C, while the red bars illustrate the expansion rates for KOH etching at 65°C.

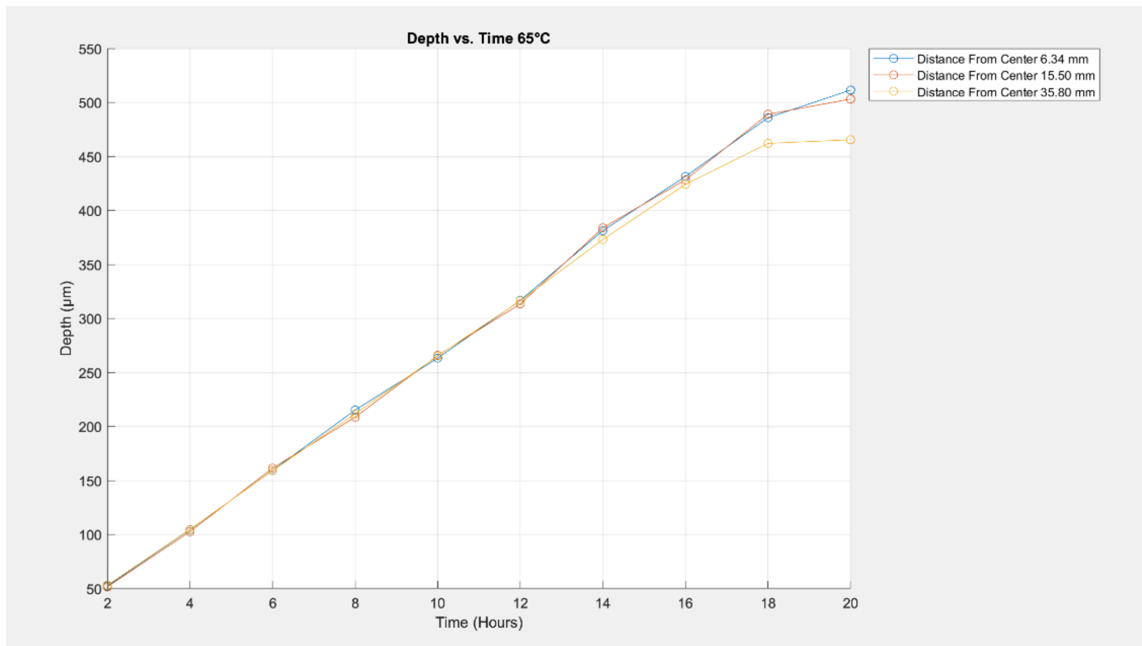

Figure 3.2.4. Average Depth for microarrays at varied distances from the wafer's center at 65°C. This figure demonstrates the variation in the average depth etch rate of microarrays.

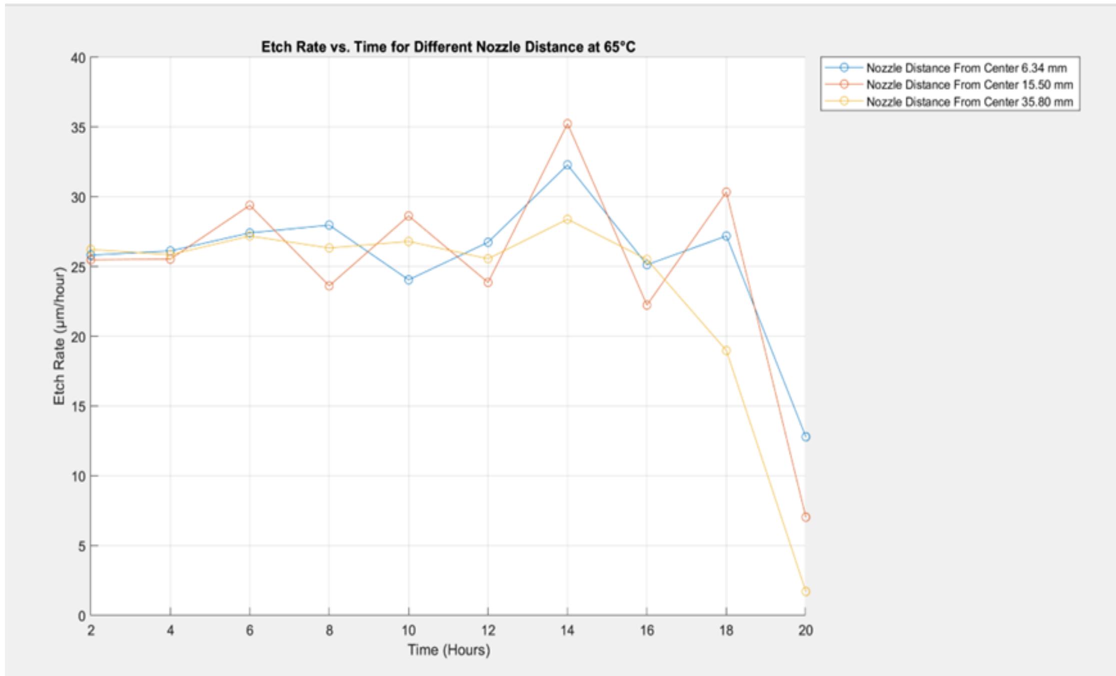

Figure 3.2.5. Average Depth etching rates for microarrays at varied distances from the wafer's center at 65°C. This figure demonstrates the variation in the average depth etch rate of microarrays.

In Figure 3.2.2, it shows that the 65°C etching exhibits large differences in nozzle sizes at the same etching time. This is because microarrays were more concentrated and closer to each other in the center of the wafer compared to microarrays on the edge of the wafer. The generation of hydrogen bubbles was also observed to be much more concentrated at the center of the wafer. The arrays in the center experienced different etch rates due to the varied distribution of hydrogen bubbles over the testing wafer. From Figure 3.2.4 and 3.25, nozzles near the center have greater etching depths and etching rates compared to nozzles on the edge.

During the KOH etching process at 65°C, a unique issue was observed. In some features near the center of the wafer, ripple-like wave patterns emerged. The sidewall surface was rough and cavity as depicted in Figure 3.2.6 (a). Due to this issue, the depth of etching and etching rate at different distances were plotted for comparison. However, from

Figures 3.2.7 and 3.2.8, plots did not show the issue was depth related. Upon examination under a microscope, as shown in Figure 3.2.6(b)(c), the affected features failed to form complete pyramids even after the silicon layer was fully etched. Moreover, the surfaces of the slanted sidewalls in these areas were exceptionally rough. Figure 3.2.6 (b) illustrates the most severe case, where the etching has exceeded the (111) plane in both the top-left and bottom-right corners. Unlike typical surface roughness, this phenomenon resulted in the formation of many angular, uneven structures on the wall surfaces.

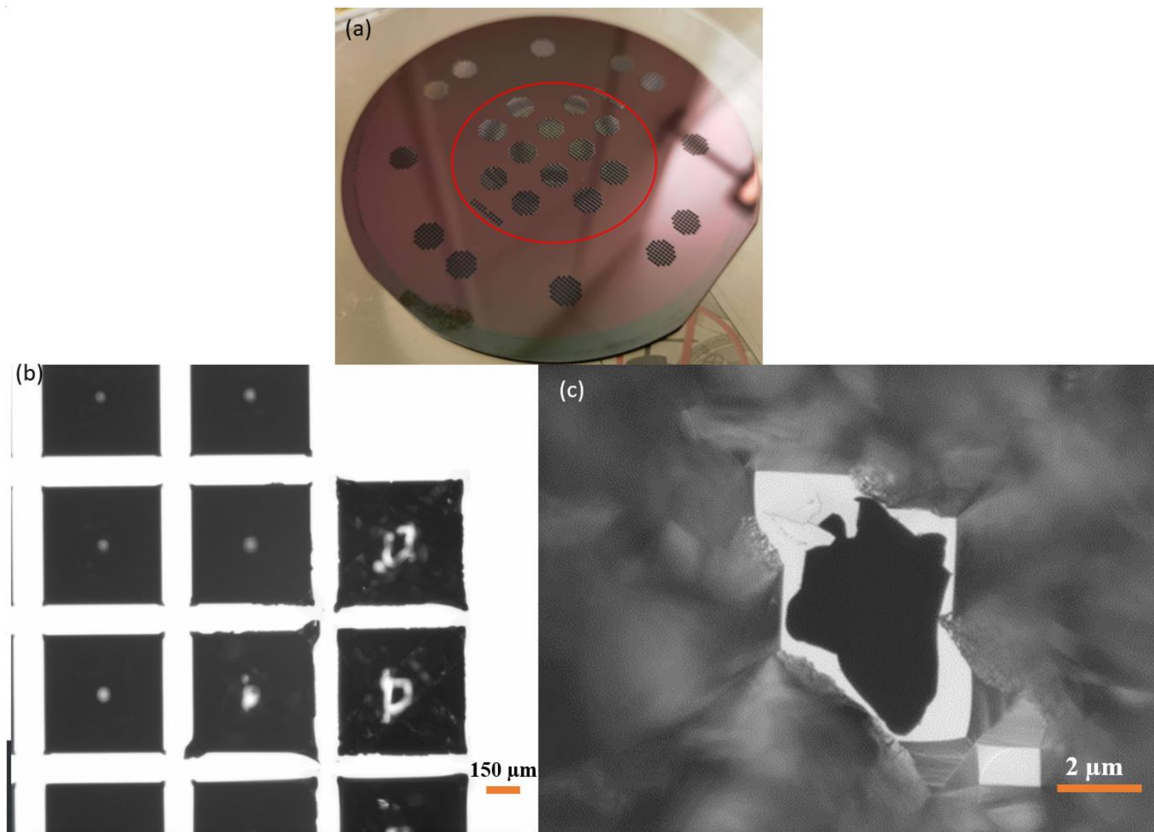

Figure 3.2.6: Anomalies Observed During KOH Etching at 65°C. (a) displays the problematic wafer at 65°C, where concentric wave patterns are visible within the red circle, discernible to the naked eye due to variations in the refraction angle and refractive index. (b) shows the appearance of the upper layer under a microscope at 2.5× magnification. (c) depicts the bottom layer as observed under 20 × magnification through the microscope

The rough surface of the sidewalls led to an incomplete formation of the pyramid structure. This roughness indicates that those regions underwent a more aggressive etching process over the (111) plane. However, the etching depth rates shown in Figures 3.2.7 and 3.2.8 suggest that areas near the center, which have a rough sidewall surface, experience a slower etching rate. Additionally, both the upper and lower layers of the nozzle displayed a slower etching rate compared to the unaffected regions near the wafer's edge, as illustrated in Figures 3.2.7 and 3.2.8. This was the first time such a phenomenon has been observed during the ultrasonic KOH etching process, which did not exhibit this behavior for 75°C and 70°C ultrasonic KOH etching. Prior to this, a similar occurrence was noted when using a magnetic stirring bar for KOH etching, with even more pronounced effects. As shown in Figure 3.2.9, the affected areas exhibited uneven, rough surfaces, with etching that has penetrated through the (111) plane. Up to this point, three ultrasonic KOH etching experiments have been conducted. Under

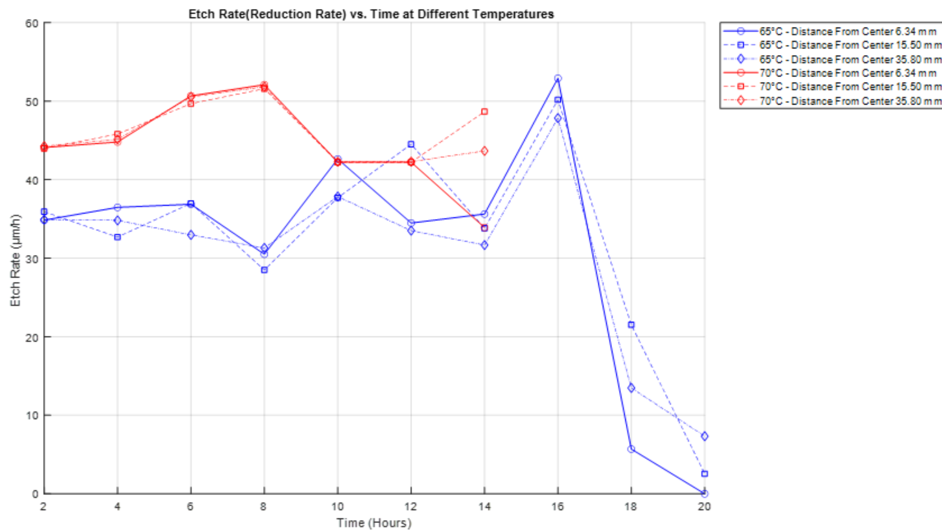

Figure 3.2.7: This figure illustrates the dimensional changes at the bottom of the nozzle over the course of KOH etching time. The blue curve represents the etching progression at 65°C, while the red curve denotes the changes observed at 70°C.

identical settings with only temperature variations, this phenomenon occurred exclusively during the etching process at 65°C.

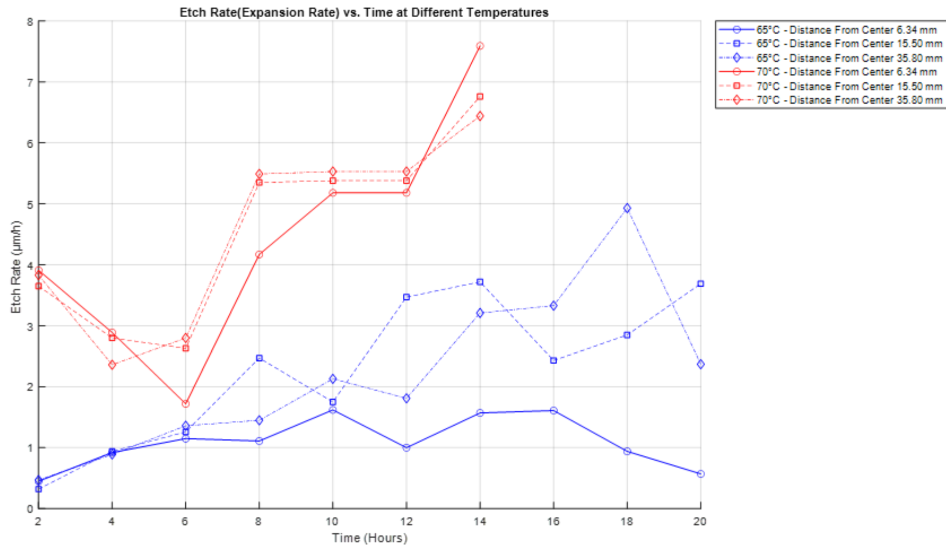

Figure 3.2.8: This figure illustrates the dimensional changes at the top of the nozzle over the course of KOH etching time. The blue curve represents the etching progression at 65°C, while the red curve denotes the changes observed at 70°C.

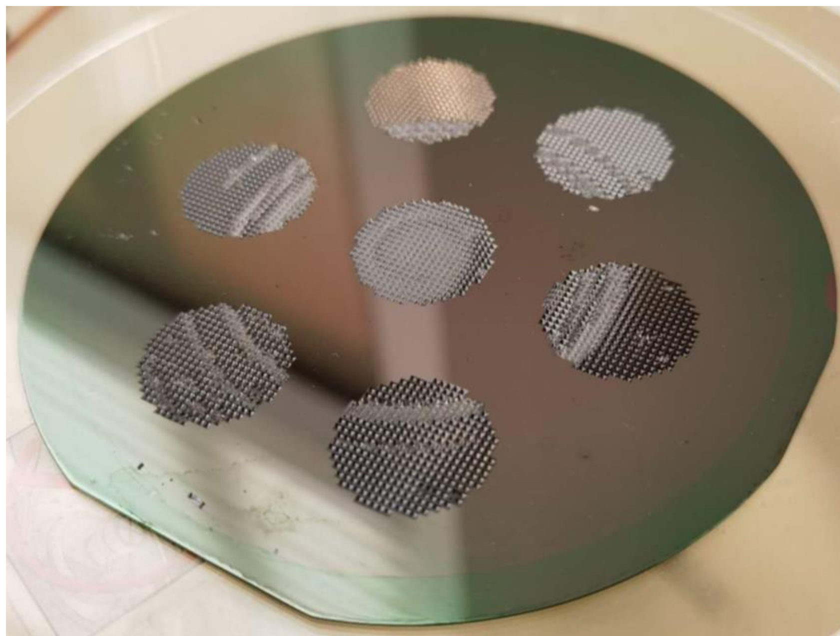

Figure 3.2.9: Ripple-patterned wafer surface, exhibiting a diffusion-like spread from the center.

3.3 Observed Issues and Possible Sources of Error

Regarding the occurrence of the irregular etching phenomenon, there is a current hypothesis. It suggests that during the RIE process, the gas used for etching within the RIE chamber might have been contaminated with residues from previous experiments. The photoresist that is slightly etched redeposits on the wafer onto the wafer, potentially leading to this observed effect. However, the issue with this hypothesis is that if the circular areas of the features are redeposited or covered with some material, the etching in these regions should be slower than in other unaffected areas. Logically, these parts should not exhibit more aggressive etching.

Another hypothesis is that the use of ultrasonics in the KOH etching process, specifically the intensity of the waves and the ultrasonic frequency, might have led to this unique ripple-pattern etching issue. However, this issue also occurred in KOH etching processes where ultrasonics were not used. Additionally, in the other two instances of ultrasonic etching at 75 and 70 ºC this problem did not arise, making this hypothesis less likely.

According to Chutani's research [18], a potential explanation for the unique etching phenomenon observed may relate to residual stress in the wafers, possibly induced during the Low-Pressure Chemical Vapor Deposition (LPCVD) processing of the nitride mask. This stress might be more pronounced in the central region of the wafers, leading to variations in etch rate observed there. However, even this hypothesis struggles to account for the drastic differences in etch rate that we have observed, which are much more significant than the small, local pitting typically seen in such processes.

Differing from the findings reported by Chutani et al. [18], where defects were only a few microns deep and primarily visible under specific microscopic conditions, the anomalies

in our study are visibly larger and detectable with the naked eye. If the factors identified by Chutani et al. were causing our observed issues, we would expect to see these defects consistently across the entire wafer, not just near the center.

Additionally, our findings do not support the hypothesis of crystal misalignment, despite our use of flat versus pre-etched featuresfor alignment. If misalignment were the primary issue, it would likely result in defects across the entire wafer. Our observations, however, are localized, suggesting the presence of other, as yet unidentified factors that are influencing the etching process.

3.4 Surface Morphology

Figures 3.4.1, 3.4.2, and 3.4.3 respectively showcase the surface characteristics of the (111) plane after etching at 75°C, 70°C, and 65°C. Due to the surface roughness at the center of the wafer from 65°C etching, all images were taken from pyramidal base size 635μm microarrays, which were in the region not affected on the wafer after 65°C etching. In Figure 3.3.1, noticeable surface undulations are observed, whereas the surface in Figure 3.4.2 appears relatively smoother, albeit with some irregularities and a few small pits. In contrast, the surface from wafer etched in the 65°C KOH bath in Figure 3.4.3 is the smoothest among the three images. Under microscopic observation, it exhibits almost no significant unevenness.

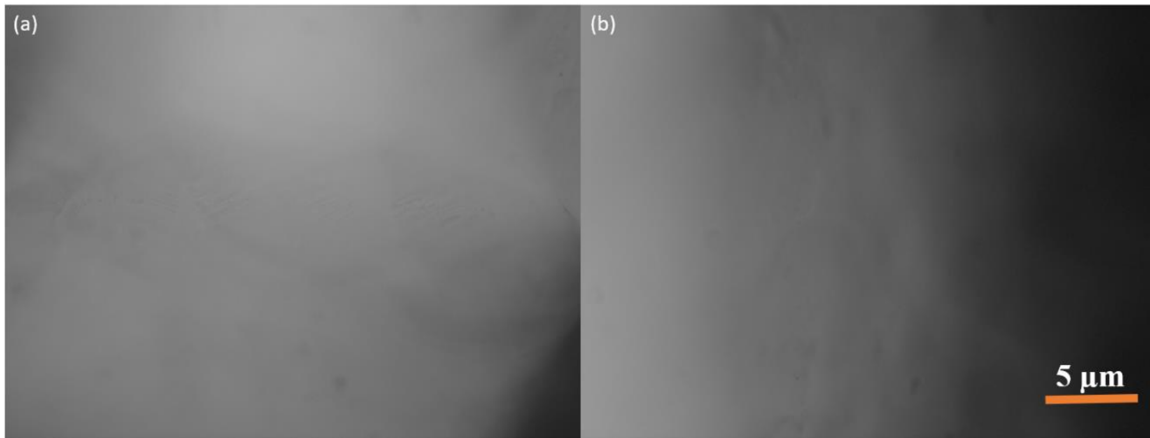

Figure 3.4.1. Surface Morphology of the Side Wall on the (111) Plane of 75ºC KOH etching. (a) in the X-direction and (b) in the Y-direction.

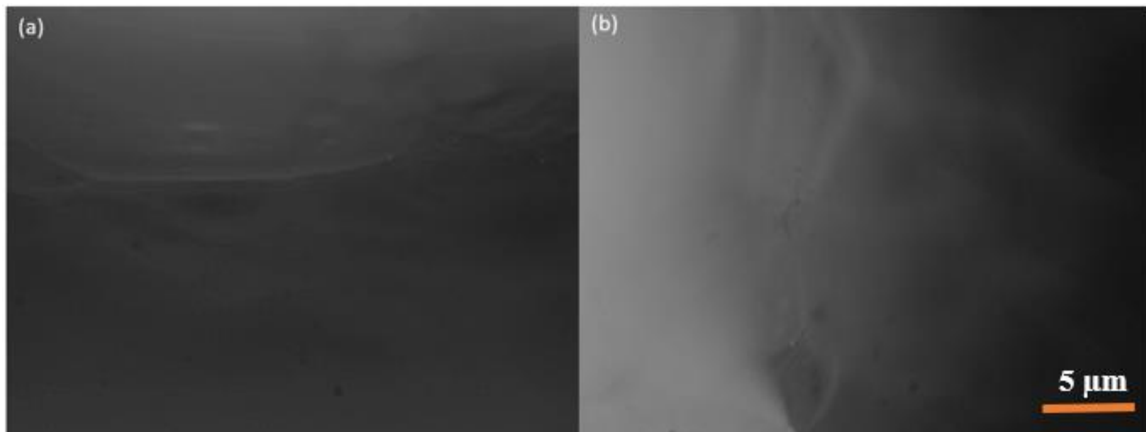

Figure 3.4.2. Surface Morphology of the Side Wall on the (111) Plane of 70ºC KOH etching. (a) in the X-direction and (b) in the Y-direction.

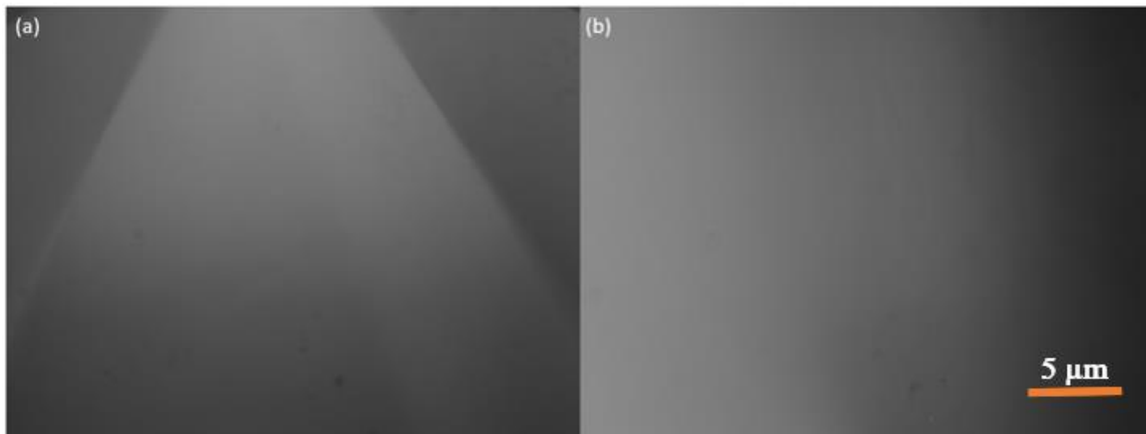

Figure 3.4.3. Surface Morphology of the Side Wall on the (111) Plane of 65ºC KOH etching. (a) in the X-direction and (b) in the Y-direction.

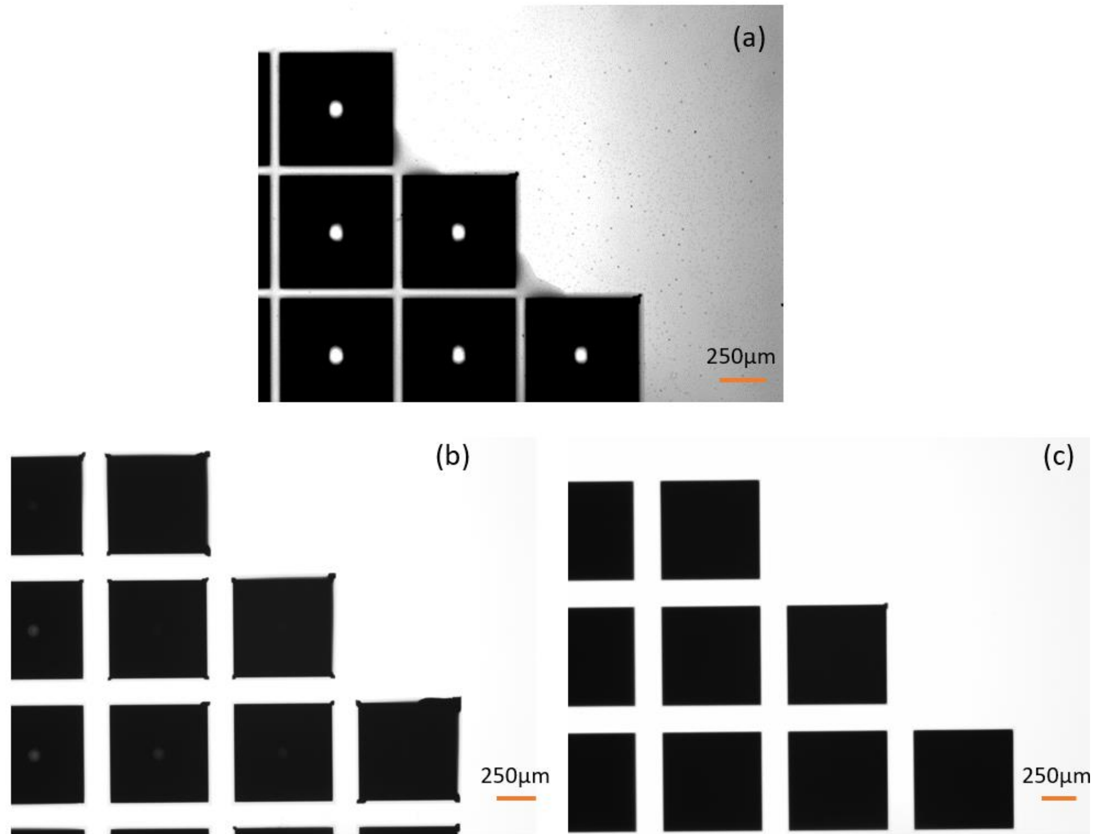

Figure 3.4.4. This figure presents the varying surface morphologies of the silicon nitride layer post-KOH etching at different temperatures for a feature size of 645μm. (a) represents the surface after the KOH etching of 75°C, (b) 70°C, and (c) 65°C.

From Figure 3.4.4(a), it is observable that the distances between the squares have become noticeably smaller. Additionally, even when focused on the silicon nitride layer, it is evident that it has not formed a complete pyramidal structure and contains numerous very small pits. On the outermost edges of the microarray, there are two apparent trapezoidal areas of excessive etching. In Figure 3.4.4(b), it is also visible that several squares in the lower-left corner have not formed complete pyramidal structures, but the situation is relatively better compared to the 75°C condition. However, it can be noted that the edges of a few squares in the upper-right corner exhibit irregular expansion areas. In contrast, in Figure 3.4.4(c), the upper surface at 65°C appears very complete. The entirely black areas indicate the formation of complete pyramidal structures, and this condition also exhibits

the smallest feature expansion. From Figure 3.4.2(c), zooming into the bottom section reveals the formation of a complete pyramidal structure, which could be observed from Figure 3.4.5.

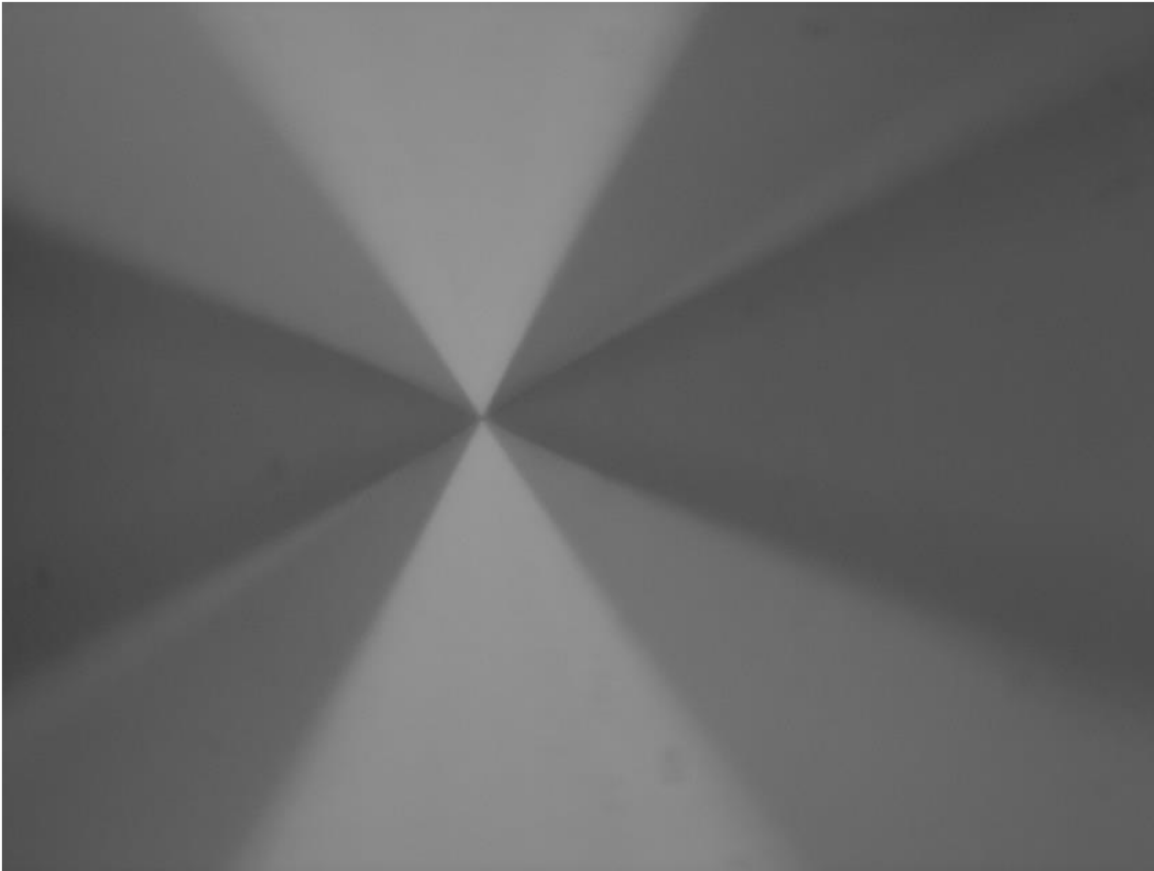

Figure 3.4.5: Pyramid Tips Resulting from KOH Etching at 65°C.

Chapter 4: Conclusions

To conclude this thesis, the exploration of ultrasonic KOH etching processes has yielded significant insights, particularly into the temperature-dependent nuances of the etching behavior. The research was primarily focused on understanding the etching dynamics at various temperatures, though the peculiarities observed at 65°C remain to be explained. Notably, the unique faceting and ripple-pattern etching issues observed at this temperature presented an intriguing anomaly, prompting a deeper investigation into the causes behind such irregularities.

The thesis posed various hypotheses for the potential causes of these features, considering factors such as ultrasonic wave distribution on the wafer during wet etching or possible chemical contamination when etching the mask layer in the RIE. While these exploratory hypotheses provided some direction, they did not conclusively explain the phenomena observed. This gap in understanding underscores the necessity for more advanced analytical approaches, such as the use of COMSOL [19] Multiphysics for simulation of the acoustic and thermal behaviors during wet etching. By modeling the temperature distribution and the effects of ultrasonic vibrations, a more comprehensive understanding of the etching process and its anomalies can be achieved. Additionally, future ultrasonic KOH etching experiments could introduce isopropyl alcohol (IPA) into the KOH solution. During the etching process, the addition of IPA is expected to effectively reduce the solution surface tension promoting release of liberated hydrogen bubbles. Theoretically, this should minimize the formation of hillocks, thereby decreasing the residence time of bubbles on the silicon substrate and increasing the surface smoothness [17].

Significantly, when devoid of the peculiar faceting and ripple-like features, the 65°C KOH etching process demonstrated superior performance. This finding is crucial, as it suggests that under optimal conditions, the 65°C etching process could potentially offer the most efficient and precise outcomes. This aspect of the research has substantial implications for the field of microfluidics and related disciplines, particular for our fabrication of nozzle microarrays, where the precision of the etching process is paramount. Understanding and harnessing the optimal conditions for KOH etching at this temperature could lead to advancements in fabrication techniques essential for developing high-precision microfluidic devices.

However, the journey through this research was marked by various technical challenges, from equipment calibration to maintaining chemical purity, each adding a layer of complexity to the experimental process. These challenges highlight the importance of methodological rigor and the need for continuous improvement in experimental design and setups.

Despite its comprehensive scope, the study is not without limitations. The specific setting of the experiments and the materials used might influence the applicability of the findings in different scenarios. Future research endeavors could aim to expand on these findings, exploring a wider range of materials and conditions.

As this thesis concludes, it is evident that while substantial progress has been made in understanding the ultrasonic KOH etching process, there remain avenues yet to be explored. Future research could delve into alternative etching chemistries, experiments with varying substrate materials (e.g., silicon with different levels of doping), and

exploration of different ultrasound settings. Such investigations could not only address the unresolved questions of this thesis but also broaden our understanding of microfabrication processes, contributing significantly to the advancement of microfluidics and allied fields.

References

[1] L. E. Murr and W. L. Johnson, “3D metal droplet printing development and advanced materials additive manufacturing,” J. Mater. Res. Technol. 6, 77–89 (2017).

[2] J. Plog, Y. Jiang, Y. Pan, and A. Yarin, “Electrostatic charging and deflection of droplets for drop-on-demand 3D printing within confinements,” Addit. Manuf. 36, 101400 (2022)

[3] Y. Lu, C. Kacica, S. Bansal, L. M. Santino, S. Acharya, J. Hu, C. Izima, K. Chrulski, Y. Diao, H. Wang, P. Biswas, J. Schaefer, and J. M. D’Arcy, “Synthesis of submicron PEDOT particles of high electrical conductivity via continuous aerosol vapor polymerization,” ACS Appl. Mater. Interfaces 11, 47320–47329 (2019).

[4] B. Joshi, J. Kaur, E. Khan, A. Kumar, and A. Joshi, “Ultrasonic atomizer driven development of doxorubicin-chitosan nanoparticles as anticancer therapeutics: Evaluation of anionic cross-linkers,” J. Drug Delivery Sci. Technol. 57, 101618 (2020).

[5] J.-W. Kim, Y. Yamagata, M. Takasaki, B.-H. Lee, H. Ohmori, and T. Higuchi, “A device for fabricating protein chips by using a surface acoustic wave atomizer and electrostatic deposition,” Sens. Actuators B: Chem. 107, 535–545 (2005).6.P. Wu, C. Noland, M. Ultsch, B. Edwards, D. Harris, R. Mayer, and S. F.

[6] Harris, “Developments in the implementation of acoustic droplet ejection for protein crystallography,” J. Lab. Autom. 21, 97–106 (2016).

[7] E. K. Sackmann, L. Majlof, A. Hahn-Windgassen, B. Eaton, T. Bandzava, J. Daulton, A. Vandenbroucke, M. Mock, R. G. Stearns, and S. Hinkson, “Technologies that enable accurate and precise nano- to milliliter-scale liquid dispensing of aqueous reagents using acoustic droplet ejection,” J. Lab. Autom. 21, 166–177 (2016).

[8] B. Edwards, J. Lesnick, J. Wang, N. Tang, and C. Peters, “Miniaturization of high-throughput epigenetic methyltransferase assays with acoustic liquid handling,” J. Lab. Autom. 21, 208–216 (2016).

[9] A. G. Fedorov and J. M. Meacham, “Evaporation-enhanced, dynamically adaptive air (gas)-cooled heat sink for thermal management of high heat dissipation devices,” IEEE Trans. Compon. Packaging Technol. 32, 746–753 (2009).

[10] H. Chen, W-l Cheng, Y-h Peng, W-w Zhang, and L-j Jiang, “Experimental study on optimal spray parameters of piezoelectric atomizer based spray cooling,” Int. J. Heat Mass Transfer 103, 57–65 (2016).

[11] W. He, Z. Luo, X. Deng, and Z. Xia, “A novel spray cooling device based on a dual synthetic jet actuator integrated with a piezoelectric atomizer,” Heat Mass Transfer 56, 1551–1563 (2020).

[12] L. E. Murr and W. L. Johnson, “3D metal droplet printing development and advanced materials additive manufacturing,” J. Mater. Res. Technol. 6, 77–89 (2017).

[13] J. Plog, Y. Jiang, Y. Pan, and A. Yarin, “Electrostatic charging and deflection of droplets for drop-on-demand 3D printing within confinements,” Addit. Manuf. 36, 101400 (2020).

[14] J. M. Meacham, C. Ejimofor, S. Kumar, F. L. Degertekin, and A. G. Fedorov, “Micromachined ultrasonic droplet generator based on a liquid horn structure,” Rev. Sci. Instrum., vol. 75, no. 5, pp. 1347–1352,2004.

[15] L. Shan, M. Cui, and J. M. Meacham, "Spray characteristics of an ultrasonic microdroplet generator with a continuously variable operating frequency," J. Acoust. Soc. Am., vol. 150, no. 2, pp. 1300–1310, 2021.

[16] S. A. Campbell, "Fabrication Engineering at the Micro- and Nanoscale," 3rd ed. Oxford, U.K.: Oxford University Press, 2007, ISBN: 9780195320176.

[17] Pal, P., Swarnalatha, V., Rao, A.V.N. et al. “High speed silicon wet anisotropic etching for applications in bulk micromachining: a review,” Micro and Nano Syst Lett 9, 4 (2021).

[18] R. K. Chutani et al., 'Deep Wet-Etched Silicon Cavities for Micro-Optical Sensors: Influence of Masking on {111} Sidewalls Surface Quality,' J. Microelectromech. Syst., vol. 23, no. 3, Jun. 2014, doi: 10.1109/JMEMS.2013.2285575

[19] COMSOL Multiphysics, COMSOL Inc., Canonsburg, PA.

[20] L. Shan, M. Cui, and J. M. Meacham, "Spray characteristics of an ultrasonic microdroplet generator with a continuously variable operating frequency," J. Acoust. Soc. Am., vol. 150, no. 2, pp. 1300–1310, 2021.

[21] X. Chen, A. Du, K. Liang, Z. Li, M. Zhang, C. Yang, and X. Wang, "Interaction between droplet impact and surface roughness considering the effect of vibration," Int. J. Heat Mass Transf., vol. 220, 2024, Art. no. 125018.

[22] L. Shan, "Nozzle microarray fabrication process," Unpublished lab report, Aug. 29, 2021